Agricultural and Forest Meteorology 149 (2009) 1152–1160

Contents lists available at ScienceDirect

Agricultural and Forest Meteorology

journal homepage: www.elsevier.com/locate/agrformet

Modeling approaches to estimate effective leaf area index from aerial discrete-return LIDAR

Jeffrey J. Richardson [a,1], L. Monika Moskal [a], Soo-Hyung Kim [a,b,1,*]

[a] College of Forest Resources, University of Washington, Box 352100, Seattle, WA 98195-2100, United States
[b] University of Washington Botanic Gardens, University of Washington, Box 354115, Seattle, WA 98195-4115, United States

ARTICLE INFO

Article history:
Received 5 September 2008
Received in revised form 2 February 2009
Accepted 3 February 2009

Keywords:
Leaf area index
LIDAR
Hemispherical photographs
Urban forest
Modeling
Vegetation

ABSTRACT

Leaf area index (LAI) has traditionally been difficult to estimate accurately at the landscape scale, especially in heterogeneous vegetation with a range in LAI, but remains an important parameter for many ecological models. Several different methods have recently been proposed to estimate LAI using aerial light detection and ranging (LIDAR), but few systematic approaches have been attempted to assess the performance of these methods using a large, independent dataset with a wide range of LAI in a heterogeneous, mixed forest. In this study, four modeling approaches to estimate LAI using aerial discrete-return LIDAR have been compared to 98 separate hemispherical photograph LAI estimates from a heterogeneous mixed forest with a wide range of LAI. Among the four approaches tested, the model based on the Beer–Lambert law with a single parameter (k: extinction coefficient) exhibited highest accuracy ($r^2 = 0.665$) compared with the other models based on allometric relationships. It is shown that the theoretical k value (=0.5) assuming a spherical leaf angle distribution and the zenith angle of vertical beams (=0°) may be adequate to estimate effective LAI of vegetation using LIDAR data. This model was then applied to six 30 m × 30 m plots at differing spatial extents to investigate the relationship between plot size and model accuracy, observing that model accuracy increased with increasing spatial extent, with a maximum r^2 of 0.78 at an area of 900 m^2. Findings of the present study can provide useful information for selection and application of LIDAR derived LAI models at landscape or other spatial scales of ecological importance.

1. Introduction

Estimates of leaf area index (LAI), broadly defined as the total leaf surface area per unit ground surface area, but often differing in their precise definition (Asner et al., 2003), are important input parameters for a wide range of ecological models (Gower et al., 1999; Hanssen and Solberg, 2007; Melillo et al., 1993), but arriving at estimates over large spatial scales has proven difficult due to limitations in time, cost, and accuracy. LAI is commonly estimated, using theory based on the Beer–Lambert law, by hemispherical photographs, the TRAC instrument (Chen and Cihlar, 1995), or commercially available canopy analyzers such as the LAI-2000 (LI-COR Inc., Licoln, Nebraska, USA) (Gower et al., 1999), but these methods have limited applications for large areas due the time required in acquiring and processing the data.

Indirect techniques utilizing remote sensing to estimate LAI show the most promise for delivering accurate estimates at larger spatial scales. Existing techniques fall into two main categories: (1) passive optical remote sensing, which tends to be limited in the range of LAI values it can accurately estimate because of saturation at high LAI associated with the indices such as the Normalized Vegetation Difference Index (NDVI) (Gower et al., 1999; Lüdeke et al., 1991) and (2) active light detection and ranging (LIDAR) remote sensing, which has been shown to be successful on a limited range of LAI values and/or for vegetation with limited species diversity (Lim et al., 2003; Morsdorf et al., 2006; Riaño et al., 2004; Solberg et al., 2006). Most studies have derived the effective LAI (L_e), which does not correct for the non-random distribution of foliage or the presence of non-foliage elements (e.g., branches, bark) in the canopy. Indirect methods based on the Beer–Lambert law also calculate effective LAI. If the true LAI is desired, one could perform corrections, and these methods have been previously described in the literature (Chen et al., 1997; Leblanc et al., 2005).

Aerial LIDAR utilizes an airplane or helicopter mounted scanning laser with an integrated GPS unit to collect three-dimensional data points (Lefsky et al., 2002). The characteristics of the final dataset depend on various parameters such as the height of the aircraft,

* Corresponding author at: UW Botanic Gardens, College of Forest Resources, University of Washington, 3501 NE 41st Street, Box 354115, Seattle, WA 98195-4115, United States. Tel.: +1 206 616 4971; fax: +1 206 685 2692.
E-mail address: soohkim@u.washington.edu (S.-H. Kim).
[1] These authors contributed equally to this work.

0168-1923/$ – see front matter © 2009 Elsevier B.V. All rights reserved.
doi:10.1016/j.agrformet.2009.02.007

radius of the LIDAR laser beam, scanning nadir angle, and post-processing equipment. Large footprint, full-waveform LIDAR utilizing the SLICER instrument has been shown to be capable of estimating LAI in Douglas-fir/Western-hemlock dominated forests (Lefsky et al., 1999), but the instrument is not yet widely available and is unable to give information to high spatial resolution at present. Small-footprint, multiple return systems are more widely available, and have been shown to be capable of estimating LAI in single-species dominated stands and/or in stands with a small range of LAI values (Lim et al., 2003; Morsdorf et al., 2006; Riaño et al., 2004; Solberg et al., 2006). These studies were performed in relatively homogeneous forests with a limited range of LAI. Each study used a different model to estimate LAI (see Section 2 for model details) suggesting that various methods may provide adequate estimates of LAI in homogenous forests for which the respective model has been calibrated. However, little is known about the performance of each method in a heterogeneous, mixed forest with a wide range of LAI values. To our knowledge, these LIDAR derived LAI models have not been evaluated against datasets other than the ones for which they were originally derived and calibrated.

The aim of the present study was to (1) obtain effective LAI estimates in a heterogeneous forest composed of multiple coniferous and deciduous species with a wide range of LAI values, (2) determine the best method for comparing LIDAR derived LAI metrics and ground-based field measurements, and (3) evaluate the modeling approaches for estimating LAI using aerial LIDAR.

2. Materials and methods

2.1. Study site

The present work was conducted at the Washington Park Arboretum (WPA) in Seattle, WA (Fig. 1). The WPA is a 93 ha forest managed by the University of Washington Botanic Gardens. The WPA is comprised of over 4000 individual species of tree or shrub, but dominated by a native matrix of Douglas-fir (*Pseudotsuga menziesii*), Western hemlock (*Tsuga heterophylla*), Western red-cedar (*Thuja plicata*), and big leaf maple (*Acer macrophyllum*). An 35 ha subsection of the WPA was used for the present work (Fig. 1c and d), consisting of areas with slopes less than 10%, not located on trails, at least 10 m from park boundaries, and away from buildings and parking lots. Within this subsection, 100 point locations were randomly located within five stratified fractional cover classes during the summer of 2007. Two locations were excluded from data collection due to the onset of autumnal leaf senescence, reducing the total number of points to 98 (Fig. 1c). At each location, 250 individual GPS points, acquired in one second intervals, were averaged using a Trimble GeoXT (Trimble Navigation Ltd., Sunnyvale, California, USA) operating in Differential GPS mode.

Six separate 30 m × 30 m plots were installed in the WPA in the summer of 2007, with two plots composed of all conifers, two all deciduous, and two mixed conifer and deciduous (Fig. 1d). A Nikon DTM 420 Total Station (Nikon Inc., Melville, New York, USA) and Trimble XR Pro GPS (Trimble Navigation Ltd.) were used to capture the geographic coordinates of the four plot corners and check for square. A 5 m × 5 m grid was set up over each plot for the purposes of obtaining effective LAI estimates that could be aggregated for plot wide estimates.

2.2. Ground estimates of LAI using hemispherical photography

Ground estimates of LAI were made using two methods: (1) hemispherical photography, and (2) a commercial plant canopy analyzer. A single hemispherical photograph was captured at each of the 98 locations. In addition, one hemispherical photograph was taken at each of the 49 grid intersections in the six 30 m × 30 m plots between June and August of 2007. All photographs were taken before sunrise, after sunset, or under uniformly overcast skies using a Nikon CoolPix 4500 digital camera (Nikon Inc.) leveled on a tripod 1 m above the ground. Hemispherical

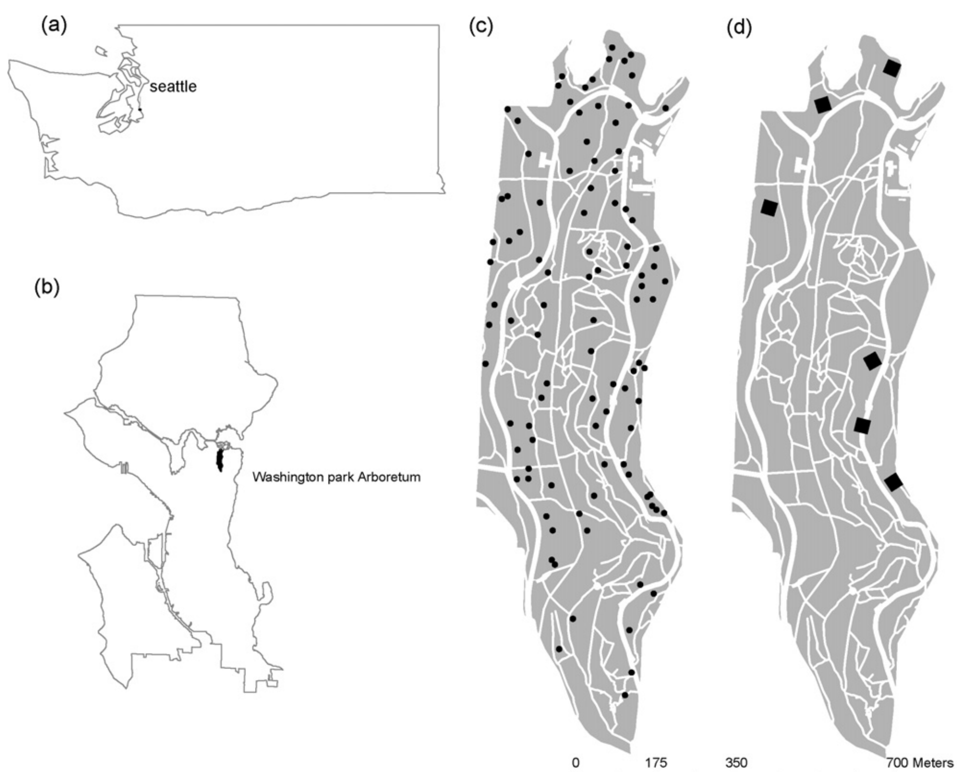

Fig. 1. (a) The state of Washington, with the city of Seattle shown by the dotted circle, (b) the city of Seattle with the WPA in black, (c) the WPA and the 98 points, and (d) the WPA and the six 30 m × 30 m plots.

photographs were obtained utilizing the methodology of Zhang et al. (2005) to find the optimum exposure time. Photographs were processed using the Digital Hemispherical Photography (DHP) software (Leblanc, 2006), which breaks the photograph into ten annulus rings, with each ring corresponding to 9° of zenith angle, beginning with 0–9° at ring one. Rings 9 and 10 were excluded from all analysis due to the influence of topography on the LAI estimates. Eight different LAI estimates were obtained using DHP for each photograph, corresponding to the inclusion of ring one, ring one and two, and so on until the eighth estimate included rings one through eight. These estimates were obtained in order to find the best relationship between the conical view of the hemispherical photograph and LIDAR metrics obtained from a cylinder, as has been performed previously (Morsdorf et al., 2006). As noted in the introduction, the photographs estimate effective LAI, and in this study, were not corrected to find the true LAI. The LIDAR based estimates would likely require the same correction factors as the ground-based estimates.

2.3. Ground estimates of LAI using the LAI-2000

Estimates using a commercial plant canopy analyzer (LAI-2000, LI-COR, Inc., Lincoln, Nebraska) were obtained at each of the 98 points under the same sky constraints as the hemispherical photographs. Above canopy readings were taken by installing a 45° viewcap and bringing the instrument into an open area, as only one instrument was available. The viewcap allowed the reading to be taken in areas with smaller canopy gaps, as the sensor rings needed to be exposed to open sky conditions in a much smaller field of view. After an above canopy reading was obtained, the instrument was quickly brought to the point location where eight readings were taken in 45° increments. A final above canopy reading was then taken and averaged with the first in order to reduce error caused by changes in sky conditions. The LAI-2000, like the hemispherical photographs, produces estimates of effective LAI.

2.4. Interpolation of LAI at 30 m × 30 m plots

In order to arrive at plot level estimates that could be easily subdivided into smaller spatial areas, the 49 individual hemispherical photograph LAI estimates for each 30 m × 30 m plot were interpolated to a raster using the Inverse Distance Weighted (IDW) function available in ArcGIS 9.2 (ESRI, Redlands, California, USA). The interpolation allowed the 30 m × 30 m plots to be subdivided into smaller areas where individual mean LAI estimates could be calculated. IDW interpolation was compared to Spline and Kriging methods by printing graphical representations of the surfaces and comparing them to the actual stands, and IDW was found to produce a more accurate surface reflecting the natural LAI variation in the plots.

2.5. LIDAR data acquisition and processing

LIDAR coverage was obtained over the WPA on August 31st, 2004 using an Optech ALTM 30/70 laser scanner (Optech Inc., Vaughan, Ontario, Canada) at an elevation of 1200 m above ground with a maximum scan angle of ±10° from nadir. The scanner classified the LIDAR returns into 1st, 2nd, 3rd, and 4th, as well as denoting when returns were the last return. The raw LIDAR data was processed using Fusion software's ClipData feature (McGaughey, 2007) to normalize the vegetation heights above a constant ground elevation using a ground model previously developed from the LIDAR data. This produced a dataset where the height (z values) for each point represented the true elevation of that point above ground level.

2.6. LIDAR metrics and LAI models

For each of the 98 plots, cylindrical LIDAR point clouds of 2.5, 5, 10, 15, 20, and 25 m radius were extracted. Within each of these cylinders, various metrics were calculated in order to provide the variables for the models tested. The number of canopy returns above 2 m in elevation (R_c), the number of ground returns below 2 m (R_g), the mean elevation of all returns (E_m), the fraction of canopy returns over total returns (f_c), and the fraction of ground returns over total returns (f_g) were computed. Some metrics used in Lefsky et al. (1999) including closed gap volume (V_{c_gap}), filled canopy volume (V_{c_fill}), and canopy classes (C_c) could not be derived because full-waveform LIDAR was not available. Therefore, to approximate the Lefsky et al. (1999) model, a canopy volume metric (V_c), was derived by creating a Triangular Irregular Network (TIN) surface from the maximum height of the LIDAR points using ArcGIS 9.2. V_c was estimated using the surface volume tool in ArcGIS 9.2. The tool calculates the volume between the TIN canopy surface and the ground surface determined by the ground model. All abbreviations used in the paper are listed in Appendix A.

The four models investigated in this paper estimate L_e as a function of E_m (Model A), V_c (Model B), f_c (Model C) or natural log of f_g (Model D) (Table 1). Relevant information for these models including the reference, range of LAI values used in the reference, the forest type, and the original or modified modeling approach is summarized in Table 1.

2.7. Statistical analyses

Statistical analyses were performed using R version 2.6.2 (http://www.r-project.org/) or SAS NLIN procedure (ver. 9.2, SAS Institute, Cary, North Carolina). Simple linear regression analysis was performed between the 98 hemispherical photograph L_e estimates and 98 LAI-2000 estimates. Root mean square error (RMSE) was calculated according to the methodology in Kobayashi and Salam (2000) and hemispherical photograph estimates, which were the better predictors of LAI (see Section 3), were then used in subsequent analyses. It was necessary to determine the best LIDAR cylinder radius and hemispherical annulus ring combination as has been previously performed (Morsdorf et al., 2006; Riaño et al., 2004). The best fit model, determined by simple linear regression, was first selected by choosing a cylinder radius of 15 m, chosen based on previous studies (Morsdorf et al., 2006; Riaño et al., 2004), and all eight hemispherical photograph annulus rings. This best fit model (see Section 3) was then used to obtain coefficients of

Table 1
Summary of different modeling approaches to estimate LAI from aerial LIDAR. Model specific empirical parameters are denoted as α and β for each model. Note that Lefsky et al. (1999) approach utilizes full-waveform LIDAR. All others assume discrete-return LIDAR. The modified modeling approach used in this study to best approximate the four models is given, as well as letter used to identify the models in the text. Model Variables are described in Appendix A.

Model	Source	LAI range	Forest type(s)	Original form	Modified form
A	Lim et al. (2003)	0.5–4	Sugar maple/yellow birch	$L_e = \alpha + \beta E_m$	–[a]
B	Lefsky et al. (1999)	0–14	Douglas-fir/Western hemlock	$L_e = \alpha + \beta(V_{c\text{–}fill} - V_{c\text{–}gap} - C_c/H)$	$L_e = \alpha + \beta V_c$
C	Riaño et al. (2004)	0 to ≈3	Pyrenean oak and Scots pine	$L_e = \alpha + \beta f_c$	–[a]
D	Solberg et al. (2006)	0–1.6	Scots pine	$L_e = -\beta \ln(R_g/R_t)$	–[a]

[a] The original model was used without modification.

Table 2
Performance of modeling approaches to estimate LAI against hemispherical photograph L_e estimates. Model specific empirical parameters are denoted as α and β for each model. Note that Model B is an approach modified from Lefsky et al. (1999) for discrete-return LIDAR data (see text for details). S.E. represents one standard error (n = 98).

Model	Parameter estimates		r^2
	α (S.E.)	β (S.E.)	
A	0.630 (0.265)	0.220 (0.0229)	0.49
B	0.746 (0.245)	6.55×10^{-3} (6.50×10^{-4})	0.51
C	−0.992 (0.323)	0.0584 (0.00459)	0.63
D	–	2.097 (0.0665)	0.66

determination (r^2) from the simple linear regressions of the six different LIDAR cylinder radii (2.5, 5, 10, 15, 20, and 25 m) and eight different hemispherical photograph annulus ring combinations (1, 1–2, 1–3, 1–4, 1–5, 1–6, 1–7, 1–8). This radius and annulus ring combination was then used in all subsequent analyses. Each computed LIDAR metric was then analyzed using simple linear regression of the hemispherical photograph LAI estimates taken at each of the 98 points.

To evaluate the relationship between spatial extent (and thus number of LIDAR points used to compute the metrics) and predictive accuracy, the 30 m × 30 m plots were subdivided into smaller quadrilateral areas: 15 m × 30 m, 15 m × 15 m, and 7.5 m × 7.5 m. LAI was predicted for each of these areas using the best model chosen by the process above, and those estimates were compared to the average LAI determined from the mean interpolated raster values for that same spatial extent.

2.8. Creation of LAI map

The best model chosen was used to create an effective LAI map for the portion of the WPA used in this study (see Fig. 1). The spatial analyst extension for ArcGIS 9.2 was used to create a raster map of effective LAI using model parameters from Table 2.

3. Results

3.1. Determination of best indirect method

Comparisons between hemispherical photography and the LAI-2000 showed good correlation (Fig. 2, r^2 = 0.804), although the LAI-2000 produced larger estimates at low L_e values, while hemispherical photographs produced larger estimates at high L_e values. In order to determine which of the two methods of L_e estimation would be best correlated to the LIDAR metrics, the LAI-2000 and hemispherical photograph L_e estimates were compared to each of the different models for estimating L_e from LIDAR. In all cases, hemispherical photographs exhibited consistently higher correlations, and thus hemispherical photographs estimates were used for all subsequent analyses (data not shown).

3.2. Determination of best LIDAR cylinder radius and hemispherical photograph annulus ring combination

Model D performed best in the initial linear regression using all eight annulus rings and a cylinder radius of 15 m. Several data points in very dense canopy did not yield any ground returns at 2.5 and 5 m cylinder radii, and, these were excluded because of the logarithmic transformation used in the Model D. The series of simple regressions found the 10 m segment radius and the annulus ring 1–7 combination to be the best correlated (r^2 = 0.67), and this combination was used for all subsequent analyses (Fig. 3).

3.3. Comparisons of LIDAR based LAI estimation models

Regressions of ground-based L_e on the predictions of all four models were highly significant ($p < 0.01$), indicating their reasonable performance (Table 2 and Fig. 4). Models A and B showed similar results, with error quickly increasing at LAI values larger than 2 (Fig. 4a and b). Although Model C showed good correlation at low LAI values, its predictions deviated considerably from ground-based estimates in a non-linear fashion resulting in underestimation when LAI values were high. Model D was most highly correlated to the ground-based hemispherical photograph estimates of L_e (r^2 = 0.665) with lowest residual errors (RMSE = 0.994).

3.4. The relationship between spatial extent and model accuracy

Model D parameterized as in Table 2 was used to predict L_e at the six 30 m × 30 m plots. Individual estimates were obtained at each 30 m × 30 m area per plot, two 30 m × 15 m areas per plot, four 15 m × 15 m areas per plot, and sixteen 7.5 m × 7.5 m areas per plot. Fig. 5 shows the comparison of those predictions to the

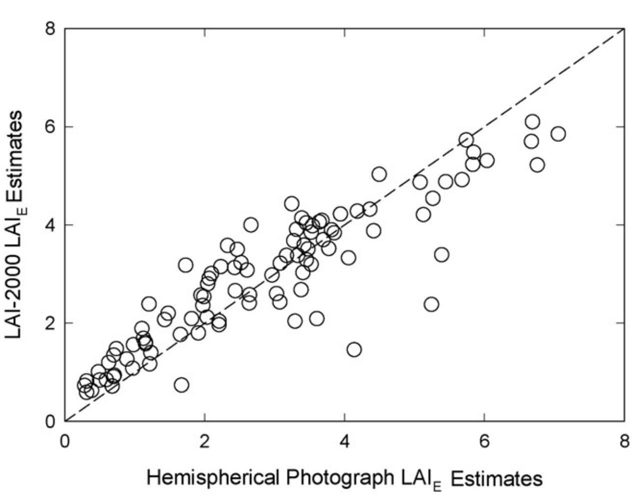

Fig. 2. Comparison of hemispherical photograph effective LAI (LAI$_E$) estimates and LAI-2000 estimates at the 98 plots within the Washington Park Arboretum. One to one relationship shown by the dotted line.

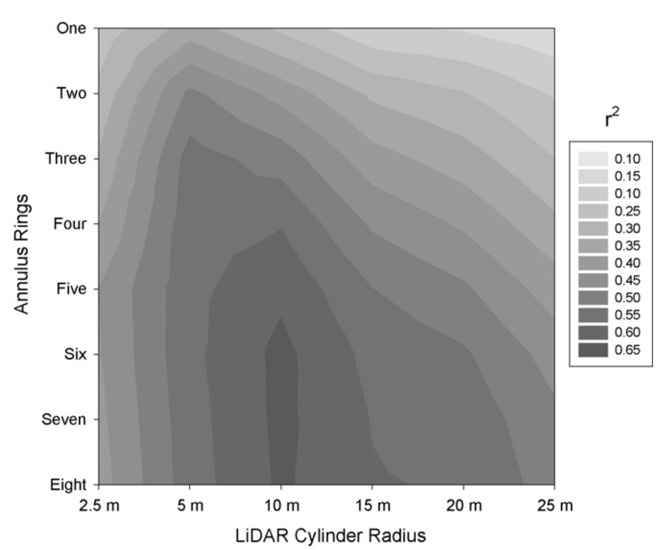

Fig. 3. Contour plot of r^2 resulting from simple linear regressions of Model D (with intercept included) at differing annulus rings and LIDAR cylinder radii at 98 points in the Washington Park Arboretum.

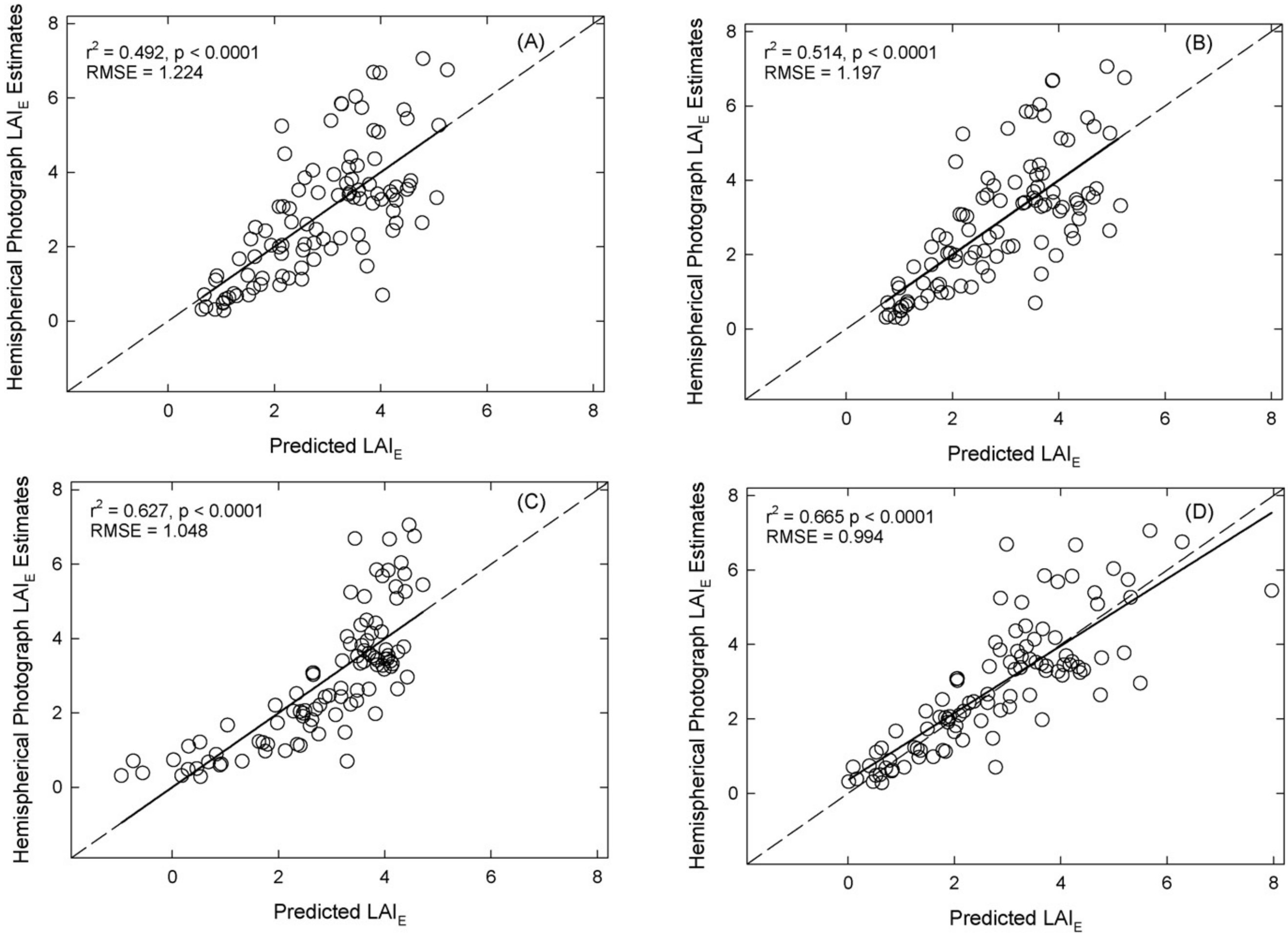

Fig. 4. Model performance based on a simple linear regression of predicted values of parameterized Models A–D against ground-based estimates from hemispherical photographs. In each graph, the dashed line represents the 1:1 relationship, and the solid line is the best fit ($n = 98$).

interpolated L_e estimates for each area. At the smallest spatial extents, several of the subplots contained no ground LIDAR returns, and were excluded from the analysis. The coefficient of determination (r^2) was also calculated for each of the four spatial extents by performing simple linear regressions of the model predictions and the interpolated L_e estimates (Fig. 5). Because of the omission of several subplots at the smallest spatial extent due to presence of no ground returns, the coefficient of determination is likely an overestimate for the 7.5 m × 7.5 m areas. Predictive accuracy of the model increased with increasing spatial extent (Fig. 5 inset).

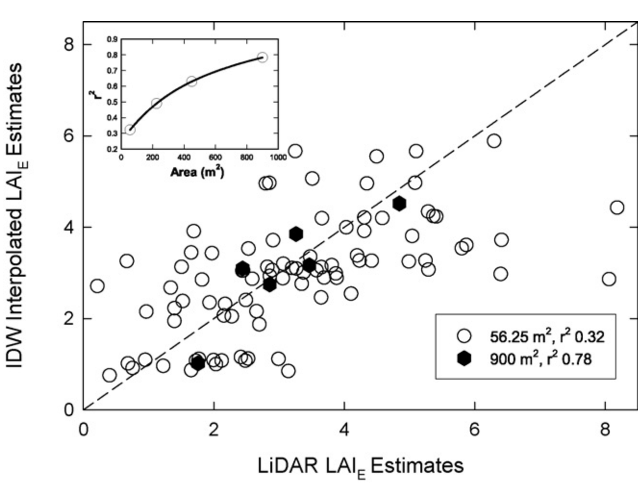

Fig. 5. Prediction of the parameterized Model D at six 30 m × 30 m plots in the WPA. Predictions are made at four spatial extents, with two spatial extents shown in the main plot. The relationship between the four spatial extents and the correlation coefficient is shown in the inset graph.

4. Discussion

4.1. The relationship between LIDAR cylinder radius and hemispherical photograph annulus rings

The best correlated combination of LIDAR radius and hemispherical photograph annulus ring combination closely matches what has been previously found (Morsdorf et al., 2006; Riaño et al., 2004). Attempting to correlate L_e estimates based on gap fraction estimates from radiation captured from a conical area of the sky to a cylindrical LIDAR point cloud will likely result in some errors. In a heterogeneous forest such as WPA, this error is magnified as there is a high probability that areas at the far edge of the photograph's conical view will be different than the areas in the middle which more closely relate to the cylindrical LIDAR point cloud. This error contributes to the residual errors seen in Fig. 4, and underscores the inherent difficulty in obtaining precise indirect L_e estimates. While indirect ground-based methods such as hemispherical photographs and the LAI-2000 are effective at obtaining stand level L_e from multiple areas within a stand, LIDAR based methods are likely to be more powerful for obtaining precise estimates for specific spatial extents.

The cost effectiveness and relative speed at which hemispherical photographs can be acquired will continue to make them an attractive method for obtaining ground-based estimates of L_e, but the inherent error of matching a cone to a cylinder suggests that the upper bound of potential correlation between photographs and LIDAR may have already been reached. Future studies should concentrate on methods to arrive at the true LAI within the cylindrical space around a point. One promising method is to use simulated forests to explore the limitations of LIDAR (Goodwin et al., 2007; Holmgren et al., 2003).

4.2. Comparison of LAI estimation methods

As noted in the introduction, ground-based indirect LAI estimation may be categorized into the two groups: allometric methods and methods based on the Beer–Lambert law. Allometric methods tend to be applicable for a single species in a single geographical area, and when allometric equations are applied to trees outside of the calibration range, their accuracy decreases (Gower et al., 1999). The two models based on biophysical variables, Model A based on canopy height (E_m) and Model B model based on canopy volume (V_c), experience rapidly increasing residual error at L_e values greater than 2 (Fig. 4a and b). If the WPA was dominated by a single species, these models might have predicted relatively accurate values of L_e, but since it is distinctively heterogeneous, the relationship between volume and height and L_e differs greatly amongst species, accounting for the large residual errors. While this suggests that these models may be appropriate to predict L_e in homogenous forests, they may still require an independent calibration process using ground-based LAI estimation methods in order to estimate empirical parameters to be applied at larger spatial scales.

Monsi and Saeki (2005; note this reference is an English translation of the original article published in German in 1953) demonstrated that light attenuation in plant canopies could be represented by the Beer–Lambert equation of light extinction as a function of LAI as follows:

$$I = I_0\, e^{-kL} \tag{1}$$

where I is the below canopy light intensity, I_0 is the above canopy light intensity, L is the leaf area index, and k is the extinction coefficient. The extinction coefficient (k) is determined by a number of factors including leaf angle distribution, radiation type and direction, and canopy structure and clumping (Breda, 2003). The leaf area index (L) can be then obtained from above- and below canopy radiation measurements and known k using Eq. (2) (Breda, 2003; Solberg et al., 2006):

$$L = -\frac{1}{k}\ln(I/I_0) \tag{2}$$

Since the Eq. (1) represents the probability a beam reaches the canopy at depth of L, a simple analogy to this relationship can be established between the LIDAR ground returns (R_g) and total returns (R_t) as follows:

$$R_g = R_t\, e^{-kL_e} \tag{3}$$

This relationship is clearly conserved in our data as a function of ground-based L_e (determined by the hemispherical photographs) with an estimate of k = 0.485 with an approximated 95% confidence interval between 0.45 and 0.52 (Fig. 6). The extinction coefficient in a canopy with a spherical leaf angle distribution is approximated by $0.5/\cos\theta$ where θ is the zenith angle of the incoming radiation (Jones, 1992). The effect of zenith angle may be ignored when the LIDAR scanning angles are small (e.g., $<10^\circ$ as used in this study) (Morsdorf et al., 2006). Hence, it can be seen that the estimated range of k in this study coincide with the theoretical estimate of k for a canopy with spherical leaf angle distribution for vertical beams. For its theoretical robustness and simplicity, the k value assuming a spherical leaf angle distribution has been widely used in key vegetation models for simulating primary productivity and associated ecosystem and global processes (e.g., de Pury and Farquhar, 1997). When scattering is considered this value tends to decrease slightly (Goudriaan, 1988; de Pury and Farquhar, 1997). It is not inconceivable that the foliage distribution in a mixed heterogeneous forest such as WPA follows the spherical leaf angle distribution. Studies have found that different forest types commonly exhibit foliage distribution corresponding to a spherical distribution and that significant deviations from this theoretical distribution are not common (Chen et al., 1997; Hyer and Goetz, 2004; Leblanc and Chen, 2001). This provides theoretical background for applying our estimate of k or simply that of the spherical leaf angle (i.e., 0.5) to estimate LAI of vegetation using LIDAR if the vegetation is deemed to follow the spherical leaf angle distribution. The effective LAI of a canopy with spherical foliage distribution can be approximated by Eq. (4) that is similar to model D:

$$L_e = -\frac{1}{k}\ln(R_g/R_t) \approx -\frac{\cos\bar{\theta}_{lidar}}{0.5}\ln(R_g/R_t) \tag{4}$$

Here $\bar{\theta}_{lidar}$ represents mean LIDAR scanning angle. For plant canopies exhibiting strong deviations from the spherical foliage distribution, a leaf angle distribution function (e.g., beta function) can be applied to augment this relationship for other leaf angle distributions such as ellipsoidal, horizontal, and vertical leaves (Jones, 1992; Wang et al., 2007).

The modeling approach based on the Beer–Lambert law has several benefits compared to the allometric models. In addition to the fact that this approach resulted in the best overall performance in the present study with highest r^2 and lowest RMSE (Table 2 and Fig. 4d), it does not necessarily require an independent model calibration as discussed above. In addition, there is a body of literature describing the extinction coefficient of various forest types (Monsi and Saeki, 2005; Pierce and Running, 1988; Thomas and Winner, 2000). Note that caution is needed to directly translate these empirical k values for LIDAR data because LIDAR resembles beam radiation while those empirical k values might have been derived from both direct and diffuse radiation. Solberg et al. (2006) found the extinction coefficient derived using aerial LIDAR to be approximately 0.7 for Scots pine canopy while their k values estimated from ground-based LAI measurements were 0.51 and 0.44 which are close to the theoretical value (=0.5) and similar to the LIDAR derived k value (=0.485) found in this study. The

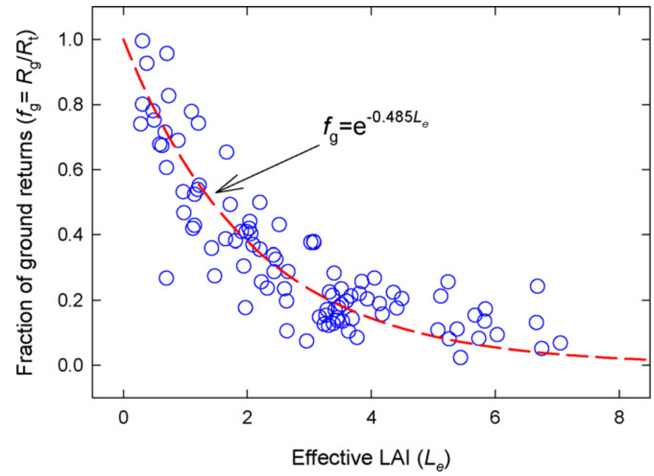

Fig. 6. Relationship between ground-based effective LAI estimates and the fraction (f_g) of LIDAR ground returns (R_g) over total returns (R_t). The red dashed line represents the model based on the Beer–Lambert's law.

differences in LIDAR derived k values from this study and the Solberg et al. (2006) study are likely a result of (1) different vegetation types, (2) differences in the range of LAI in each study, and (3) the different sensors, flying heights, and scanning angles used in each study. Separating the effects of those factors will be difficult, and a potential source of future research. A practical solution to producing L_e estimates from LIDAR in areas with no ground-based data may be to use the theoretical projection value of 0.5 for a spherical foliage distribution as shown in Eq. (4). This is a key benefit of the method following the Beer–Lambert law over the allometric-based methods, where model parameters cannot be easily estimated.

Another noteworthy approach to estimate LAI using discrete-return LIDAR has been developed by Morsdorf et al. (2006). This approach applies a LAI proxy defined as the ratio between canopy first returns and the sum of canopy single and canopy last returns to represent foliage density in the canopy, and multiplies this proxy by fractional cover to derive L_e. This method, however, was not compared in this study because the pulse duration data which can be used to test data transferability between the LIDAR instruments for computing the LAI proxy were unavailable in the dataset used in the present study.

One of the limitations of utilizing the Beer–Lambert law is that it produces estimates of effective LAI and must be corrected if true LAI is required (Chen et al., 1997). Applying multiple correction factors for the many different species in a heterogeneous forest is not realistic if one is attempting to estimate LAI for very large spatial scales, and further research is necessary to examine whether clumping indices and the ratio of stem to foliage can be directly estimated from aerial LIDAR. LIDAR intensity values present a potential source of data from which to differentiate foliage returns from bark/wood returns and have already proved effective at species classification (Andersen et al., 2005). Different objects reflect differing wavelengths of light differently, and this is the basis of most optical remote sensing. The wavelength of the laser used would have a large effect on any model developed using this technique, and perhaps the best solution would be to develop a LIDAR system that uses multiple wavelengths of lasers. A system utilizing red and near infrared lasers would be a reasonable choice as the two wavelengths exhibit such different reflectance in vegetation canopies.

4.3. *The saturation at high LAI and its relationship to other methods of remotely sensing LAI*

Although the modeling approach based on the Beer–Lambert law (Eq. (4)) was the best method for estimating L_e from aerial discrete-return LIDAR in the WPA, residual error still increased with increasing LAI. There are two likely causes for this behavior. First, the error associated with comparing the conical view of the hemispherical photograph to the cylindrical LIDAR point cloud will likely increase with increasing LAI. At high LAI, small differences in gap fraction can lead to large changes in LAI derived from hemispherical photographs. There were many point locations where dense forest patches were bordered by open areas due to the heterogeneous nature of the WPA. In these areas, the LIDAR cylinders captured only dense vegetation, while open sky at the edges of the photographs increased the gap fraction, leading to error. The opposite occurred in open areas ringed by dense vegetation. Secondly, because the model is comparing canopy returns to ground returns, the model loses accuracy in areas where few laser pulses penetrate the canopy producing few ground returns. Using a 10 m cylinder radius, none of the 98 points contained only canopy returns, but there were smaller areas within those cylinders that contained very dense vegetation below which there were no ground returns. When there is no ground returns (R_g), the model as in Eq. (4) fails. This saturation issue is also found in satellite based remote sensing using the Normalized Difference Vegetation Index (NDVI) (Wang et al., 2005). The NDVI is driven by the difference in reflectance between vegetation and ground, and when vegetation reaches a certain density, around a LAI of 3 (Lüdeke et al., 1991), this index no longer changes because the soil is mostly covered by vegetation. A similar saturating pattern is observed with LAI estimates based on LIDAR in the present study. As the gap fraction decreases, the probability of an individual laser pulse penetrating through a gap and reflecting off the ground with enough energy to be recorded by the laser scanner decreases exponentially. Hence, when the proportion of R_g is plotted against hemispherical photograph L_e estimates (Fig. 6), a curvilinear relationship develops, showing a flattening pattern over L_e greater than three. Using Model D to create a map of LAI for the WPA also highlights the saturation problem. When a 3 m pixel size is used, chosen to create a high resolution map (Fig. 7a), significant portions of the WPA contain pixels with no ground returns, producing gaps where no LAI estimate could be attained due to the logarithmic transformation in Model D. In order to obtain a continuous map with the smallest possible pixel size, it was necessary to increase the pixel size to 14 m (Fig. 7b). This tradeoff in map resolution could be a major problem if the final application of the LAI estimates require very fine resolution, such as may be desired in an urban forest where property lines and heterogeneous canopies are the norm.

While this type of model failure can be prevented simply by setting R_g to have the minimum value of 1, the error due to this (i.e., underestimation of L_e with no actual ground returns) is likely to increase with increasing LIDAR footprint and with decreasing cylinder (or pixel) size. Thus, some possible ways to improve the precision at high LAI include (1) increasing the number of laser pulses per square meter. This may increase the likelihood that a pulse will find a gap; (2) increase the spatial extent from which one is computing the number of ground and canopy returns. Fig. 5 illustrates this effect, as at larger areas there is a greater probability that an individual laser pulse will strike a canopy gap, yielding more ground returns. As noted above, this reduces the resolution of the estimates and possibly their utility; (3) the scanning angle of

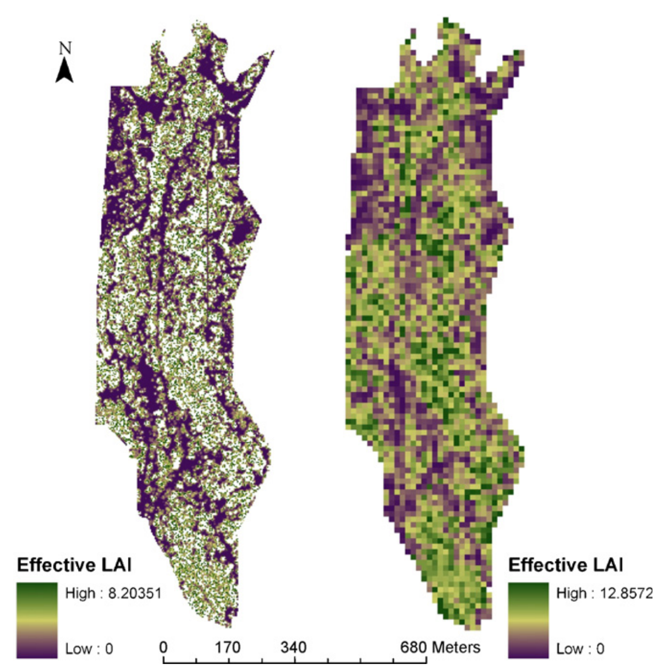

Fig. 7. Estimates of LAI_E within the area of study with (a) 3 m pixels with areas containing no ground returns shown as white and (b) 14 m pixels.

each individual laser pulse could be included as a variable in a model. Holmgren et al. (2003) showed the effect of scanning angle on canopy closure estimation, and Model D uses the inverse of canopy closure as its principle variable. At larger scanning angles, the laser beam may pass through gaps that would not be visible at very small off-nadir angles. It would be important to correct for the reduced probability of striking the ground at large off-nadir angles, though, as the path length would be increased, thus increasing the probability that light would be attenuated. If the scanning angle of each pulse is known, Eq. (4) may be used to perform this correction; (4) configure the LIDAR instrument to be more sensitive to low energy reflections. It is highly likely that laser pulses are penetrating through very small gaps, but that there is not enough reflected energy to be recorded by the scanner. As LIDAR technology matures, forestry specific instruments and calibrations should be developed to increase the sensitivity to low energy ground returns. Advances in decreasing the footprint size of full-waveform LIDAR systems show promise in overcoming this limitation.

Even with above improvements, a method using the Beer–Lambert law will be ineffective to produce reliable LAI estimates at very high LAI. Extremely dense areas of foliage that overlap will absorb all light, ensuring that no LIDAR pulses will reach the ground. In these areas, scanners that can partially penetrate foliage may provide the ultimate solution to achieving true LAI. Both long- and short-wave radiation, as well as green visible light, is transmitted through foliage, and sensors operating in these wavelengths may provide areas for future research. Similar saturating issues are inherently associated with the ground-based indirect LAI estimation based on the Beer–Lambert law. The ground-based indirect methods such as hemispherical photography measure directional gap fraction of a conical view that is a function of LAI and other canopy elements (e.g., branches and trunks). It may be argued, as Morsdorf et al. (2006) stated, that LIDAR data may provide a truer estimate of the canopy characteristics (e.g., f_c and L_e) than the ground-based indirect methods because interference by non-foliage elements and distortion of the view at low elevation angles can be minimized.

5. Conclusions

The present study investigated the applicability of various models to estimate effective LAI from aerial discrete-return LIDAR using a unique data set of ground-based LAI collected from a heterogeneous forest with a large range of LAI. The models examined in the study fall into two categories: allometric and the Beer–Lambert law based methods. A modeling approach based on the Beer–Lambert equation (Model D) as used in Solberg et al. (2006) exhibited best performance ($r^2 = 0.665$), likely due to the similar mechanistic basis of the ground-based methods used. In a heterogeneous forest, the Beer–Lambert law based approach would produce accurate predictions of effective LAI without separate calibration processes to parameterize the extinction coefficient (k). This value can be approximated to be 0.5 if the LIDAR scanning angles were narrow (i.e., near vertical) and a spherical leaf angle distribution can be assumed. Limitations on map resolution in areas of high LAI may also limit the utility of the LIDAR based estimates in some applications. Continued research to increase the applicability of LIDAR scanners for vegetation remote sensing, to examine the influence of different scanner types on LAI estimation, and to research into the possibility of deriving the clumping index and bark to foliage ratio from LIDAR data would improve the accuracy and precision of vegetation index estimation using aerial discrete-return LIDAR data.

Acknowledgements

We thank Bob McGaughey for his help with the LIDAR data processing and Akira Kato for his assistance in field data collection. This work was supported, in part, by a grant from the Royalty Research Fund at the Univ. of Washington awarded to S-HK and LMM.

Appendix A. List of abbreviations

C_c	canopy classes
E_m	mean return elevation
f_c	fractional canopy returns (i.e., R_c/R_t) or percentage of canopy returns in Model C
f_g	fractional ground returns (i.e., R_g/R_t)
H	maximum height
L	leaf area index (referred to LAI in the text)
L_e	effective leaf area index (referred to LAIE in figures)
R_c	canopy returns (returns greater than 2 m in elevation)
R_g	ground returns (returns less than 2 m in elevation)
R_t	total returns (i.e., $R_c + R_g$)
V_c	canopy volume
V_{c_fill}	filled canopy volume
V_{c_gap}	closed gap volume

Greek symbol

$\bar{\theta}_{lidar}$	mean LIDAR scanning angle

References

Andersen, H., McGaughey, R.J., Reutebuch, S.E., 2005. Forest measurement and monitoring using high-resolution airborne LIDAR. Productivity of Western forests: a forest products focus. USDA Forest Service, Pacific Northwest Research Station, pp. 109–120.

Asner, G.P., Scurlock, J.M.O., Hicke, J.A., 2003. Global synthesis of leaf area index observations: implications for ecological and remote sensing studies. Global Ecology and Biogeography 12 (3), 191–205.

Breda, N.J.J., 2003. Ground-based measurements of leaf area index: a review of methods, instruments and current controversies. Journal of Experimental Botany 54 (392), 2403–2417.

Chen, J.M., Cihlar, J., 1995. Quantifying the effect of canopy architecture on optical measurements of leaf-area index using 2 gap size analysis-methods. IEEE Transactions on Geoscience and Remote Sensing 33 (3), 777–787.

Chen, J.M., Rich, P.M., Gower, S.T., Norman, J.M., Plummer, S., 1997. Leaf area index of boreal forests: theory, techniques, and measurements. Journal of Geophysical Research-Atmospheres 102 (D24), 29429–29443.

de Pury, D.G.G., Farquhar, G.D., 1997. Simple scaling of photosynthesis from leaves to canopies without the errors of big-leaf models. Plant Cell and Environment 20, 537–557.

Goodwin, N.R., Coops, N.C., Culvenor, D.S., 2007. Development of a simulation model to predict LiDAR interception in forested environments. Remote Sensing of Environment 111 (4), 481–492.

Goudriaan, J., 1988. The bare bones of leaf-angle distribution in radiation models for canopy photosynthesis and energy exchange. Agricultural and Forest Meteorology 43 (2), 155–170.

Gower, S.T., Kucharik, C.J., Norman, J.M., 1999. Direct and indirect estimation of leaf area index, fAPAR, and net primary production of terrestrial ecosystems. Remote Sensing of Environment 70 (1), 29–51.

Hanssen, K.H., Solberg, S., 2007. Assessment of defoliation during a pine sawfly outbreak: calibration of airborne laser scanning data with hemispherical photography. Forest Ecology and Management 250 (1–2), 9–16.

Holmgren, J., Nilsson, M., Olsson, H., 2003. Simulating the effects of lidar scanning angle for estimation of mean treeheight and canopy closure. Canadian Journal of Remote Sensing 29 (5), 623–632.

Hyer, E.J., Goetz, S.J., 2004. Comparison and sensitivity analysis of instruments and radiometric methods for LAI estimation: assessments from a boreal forest site. Agricultural and Forest Meteorology 122 (3–4), 157–174.

Jones, H.G., 1992. Plants and Microclimate. Cambridge University Press, Cambridge, UK, p. 428.

Kobayashi, K., Salam, M.U., 2000. Comparing simulated and measured values using mean squared deviation and its components. Agronomy Journal 92 (2), 345–352.

Leblanc, S.G., 2006. Digital Hemispherical Photography Manual. Natural Resources Canada, Canada Centre for Remote Sensing.
Leblanc, S.G., Chen, J.M., 2001. A practical scheme for correcting multiple scattering effects on optical LAI measurements. Agricultural and Forest Meteorology 110 (2), 125–139.
Leblanc, S.G., Chen, J.M., Fernandes, R., Deering, D.W., Conley, A., 2005. Methodology comparison for canopy structure parameters extraction from digital hemispherical photography in boreal forests. Agricultural and Forest Meteorology 129 (3–4), 187–207.
Lefsky, M.A., Cohen, W.B., Acker, S.A., Parker, G.G., Spies, T.A., Harding, D., 1999. Lidar remote sensing of the canopy structure and biophysical properties of Douglas-fir western hemlock forests. Remote Sensing of Environment 70 (3), 339–361.
Lefsky, M.A., Cohen, W.B., Parker, G.G., Harding, D.J., 2002. Lidar remote sensing for ecosystem studies. Bioscience 52 (1), 19–30.
Lim, K., Treitz, P., Baldwin, K., Morrison, I., Green, J., 2003. Lidar remote sensing of biophysical properties of tolerant northern hardwood forests. Canadian Journal of Remote Sensing 29 (5), 658–678.
Lüdeke, M., Janecek, A., Kohlmaier, G.H., 1991. Modelling the seasonal CO_2 uptake by land vegetation using the global vegetation index. Tellus 43B, 188–196.
McGaughey, R.J., 2007. FUSION/LDV: Software for LIDAR Data Analysis and Visualization. United States Department of Agriculture, Forest Service, Pacific Northwest Research Station.
Melillo, J.M., McGuire, A.D., Kicklighter, D.W., Moore, B., Vorosmarty, C.J., Schloss, A.L., 1993. Global climate change and terrestrial net primary production. Nature 363 (6426), 234–240.
Monsi, M., Saeki, T., 2005. On the factor light in plant communities and its importance for matter production. Annals of Botany 95, 549–567.
Morsdorf, F., Kötz, B., Meier, E., Itten, K.I., Allgöwer, B., 2006. Estimation of LAI and fractional cover from small footprint airborne laser scanning data based on gap fraction. Remote Sensing of Environment 104 (1), 50–61.
Pierce, L.L., Running, S.W., 1988. Rapid estimation of coniferous forest leaf area index using a portable integrating radiometer. Ecology 69 (6), 1762–1767.
Riaño, D., Valladares, F., Condes, S., Chuvieco, E., 2004. Estimation of leaf area index and covered ground from airborne laser scanner (Lidar) in two contrasting forests. Agricultural and Forest Meteorology 124 (3–4), 269–275.
Solberg, S., Næsset, E., Hanssen, K.H., Christiansen, E., 2006. Mapping defoliation during a severe insect attack on Scots pine using airborne laser scanning. Remote Sensing of Environment 102 (3–4), 364–376.
Thomas, S.C., Winner, W.E., 2000. Leaf area index of an old-growth Douglas-fir forest estimated from direct structural measurements in the canopy. Canadian Journal of Forest Research-Revue Canadienne De Recherche Forestiere 30 (12), 1922–1930.
Wang, Q., Adiku, S., Tenhunen, J., Granier, A., 2005. On the relationship of NDVI with leaf area index in a deciduous forest site. Remote Sensing of Environment 94 (2), 244–255.
Wang, W.M., Li, Z.L., Su, H.B., 2007. Comparison of leaf angle distribution functions: effects on extinction coefficient and fraction of sunlit foliage. Agricultural and Forest Meteorology 143 (1–2), 106–122.
Zhang, Y.Q., Chen, J.M., Miller, J.R., 2005. Determining digital hemispherical photograph exposure for leaf area index estimation. Agricultural and Forest Meteorology 133 (1–4), 166–181.